

ANALYSIS OF TEMPERATURE DISTRIBUTION IN LASER ALLOYING OF PURE COPPER

ANALIZA PORAZDELITVE TEMPERATURE MED LASERSKIM LEGIRANJEM ČISTEGA BAKRA

**Justyna Domagała-Dubiel^{1*}, Damian Janicki², Grzegorz Muzia¹, Jakub Lisicki³,
Jacek Ptaszny⁴, Joanna Kulasa¹**

¹Lukasiewicz Research Network – Institute of Non-Ferrous Metals, Sowińskiego street 5, 44-100 Gliwice, Poland

²Welding Department, Faculty of Mechanical Engineering, Silesian University of Technology, Konarskiego Street 18A, 44-100 Gliwice, Poland

³Silesian University of Technology (Graduate Student), Konarskiego Street 18A, 44-100 Gliwice, Poland

⁴Department of Computational Mechanics and Engineering, Silesian University of Technology, Konarskiego Street 18A, 44-100 Gliwice, Poland

Prejem rokopisa – received: 2022-07-15; sprejem za objavo – accepted for publication: 2022-09-30

doi:10.17222/mit.2022.551

In many cases, the use of copper is limited by the unsatisfactory properties of its surface layer, i.e., low hardness and wear resistance. Laser surface-layer treatment may be a better alternative to other techniques used in surface engineering intended for the elements, whose high conductivity, combined with high functional properties, is required. In the present work, laser alloying of pure copper with Ni powder is performed. Thermographic measurements during the process and measurements of the melt-pool dimensions after the alloying are performed. A 3-D model of a cylindrical specimen is developed. The enthalpy-based material model involving the phase change is applied. The nickel powder is taken into account with an appropriate value of the workpiece absorptance in the heat flux boundary condition imposed in the moving laser spot area. This study utilized the ANSYS-based Simulation software. Results of the temperature simulation show acceptable agreement with the experiment. The developed model can be used to predict the temperature distribution and identify the workpiece absorptance.

Keywords: laser surface alloying, copper, temperature distribution, finite-element simulation

V mnogih primerih je uporaba čistega bakra omejena zaradi njegovih relativno slabih mehanskih lastnosti oziroma njegove nizke trdnosti ter slabe odpornosti proti obrabi. Površinska laserska obdelava bakra bi bila lahko boljše alternativa nekaterim drugim postopkom oziroma tehnikam površinskega inženiringa v primerih, ko se hkrati zahteva kombinacija njegove odlične prevodnosti z drugimi funkcionalnimi lastnostmi. V članku je opisana izvedba postopka laserskega legiranja čistega bakra z nikljevim prahom. Med postopkom so izvedli termo grafične meritve dimenzij nastalega bazenčka taline po legiranju. Izdelali so tri dimenzionalni model cilindričnega vzorca. Uporabili so entalpijski materialni model z upoštevanjem faznih sprememb. Upoštevali so dovajanje primerne količine nikljevega prahu s primerno vrednostjo absorpcije toplotnega toka pri njegovih robnih pogojih, ustvarjenih z gibanjem površine točke laserskega snopa. Študijo so izvedli s pomočjo simulacijskega programskega orodja ANSYS. Rezultati temperaturne simulacije so pokazali sprejemljivo ujemanje s praktičnimi preizkusi. Ugotovili so, da se lahko razviti model uporablja za napoved porazdelitve temperature in identifikacijo vpojnosti preizkušanca.

Ključne besede: lasersko površinsko legiranje bakra, porazdelitev temperature, simulacija z metodo končnih elementov

1 INTRODUCTION

Copper and its alloys are widely used in everyday life and in industrial practice, mainly due to their high electrical and thermal conductivity. Semi-finished products made from copper alloys with good mechanical properties and good electrical and thermal conductivity remain stable and, at high temperatures, find an ever wider application in technological solutions; they usually replace grades of pure copper and other copper alloys of inferior electrical conductivity. They are used, among others, in the production of elastic elements for electrical and electronic devices, electrodes for the resistance welding of car body sheets, tips of welding torches, trolley wires for cranes and other lifting devices, elements of relays and electric contactors, non-sparking tools used in mines and

ship engine rooms.^{1,2} However, the main problems in using copper components are its low hardness, poor abrasion and oxidation resistance, tendency to electrical erosion and atmospheric corrosion. Therefore, some attractive techniques are used in surface engineering to increase the performance of such components and to reduce their wear.³

Significant improvement of the anticorrosive properties and increase in the resistance to abrasive wear can be achieved with the application of the methods of surface metal-layer shaping. One of them is laser alloying, also known as the laser surface alloying – LSA, that is based on the introduction of alloying elements into the alloyed material.^{4,5} Mutual intense mixing of the materials occurs in the melt pool as a result of convection and gravitational movements, and a laser beam. The liquid metal rapidly cools down and solidifies as a result of a large temperature gradient at the boundary of the melted sur-

*Corresponding author's e-mail:
justyna.domagala-dubiel@imn.lukasiewicz.gov.pl
(Justyna Domagała-Dubiel)

face layer and the substrate. The surface treatment can be achieved with two techniques. The alloying material can be fed to the melt pool in a continuous powder form, i.e., in a one-step process. On the other hand, the alloying material can be pre-placed on the alloyed substrate in the form of a powder or coating layer made by plasma spraying, gas spraying or galvanizing, and then melted with a laser beam – this is called two-stage alloying.⁶

Copper and its alloys are characterized by high laser radiation reflection coefficients, posing a serious problem in the processes of laser surface treatment of these materials. Laser surface treatment is a method for improving the wear resistance. Laser cladding of Ni-based^{7,8}, Co-based⁹, Mo-based¹⁰ powder and laser alloyed layer of Cu–Fe–Al–Si¹¹ and Cr–WC powders¹² on a copper substrate have been reported. A high-power diode laser (HPDL) with direct beam transmission to the treated surface is advantageous when laser alloying materials on a Cu matrix. This is due to, among others, the multimode (even) power density distributions on the beam focus surface (the "top hat" profile). The above-mentioned advantage of HPDL lasers, in comparison to the other types of lasers, provides an additional reduction in the alloying linear energy as well as allowing a better control of the thermal conditions in the melt pool.^{13,14} To reduce laboratory experiment costs, models are often developed. In the literature, analytical methods,¹⁵ the finite-element method,^{16–18} the finite-difference method¹⁹ and the boundary-element method^{20,21} are applied.

In the present work, laser surface alloying of a Cu substrate is carried out by melting the preplaced Ni powder. The Ni powder used increases of the absorption of laser irradiation. The process is simulated to predict the temperature distribution in the workpiece. The finite-element method (FEM) simulations are performed, with usual simplifications and assumptions concerning the boundary conditions included in laser-treatment process calculations.^{22,23} The fluid flow, evaporation of the material through the surface and interaction of the material with the shielding gas are neglected. It is assumed that the liquid in the melt pool is still, although the phase change is involved with the enthalpy-based approach. The powder volume is not discretized and the model geometry is not changed during the simulation. It is assumed that the powder has an impact on the absorptance coefficient of the workpiece. The coefficient is included in the heat flux boundary condition imposed on the area of the laser spot. The absorptance of the workpiece covered with the nickel powder is identified by changing the parameter and a comparison of the simulated temperature field with the experimental data is made, including the temperature at a point close to the melt pool and the melt pool dimensions.

2 EXPERIMENTAL PART

2.1 Characterization of the materials and experimental methods

The substrate material for the laser surface treatment was copper in the form of a rod with a 50-mm diameter and 5-mm high. Copper laser alloying was performed using a HPDL, Rofin DL 020 (**Table 1**). During the process, the laser spot length was set close to the minimum possible length.

Table 1: Specifications of the Rofin DL 020

Parameter	Value
Wavelength (nm)	808–940
Power range (W)	100–2000
Focal length (mm)	82
Power density range (kW/cm ²)	0.8–36.5
Laser beam spot dimensions (mm)	1.5 × 6.6

Commercially pure Ni powder of particles with a size of below 10 μm was used as the alloying material. Before the laser surface treatment, the samples were sandblasted and then rinsed in an ultrasonic bath. The Ni powder mixed with ethyl alcohol in the form of a paste with a thickness of 120–150 μm was applied to the sandblasted copper surface and then melted by means of the laser beam. Argon was used as the shielding gas. Laser copper treatment was performed at a 2.0 kW laser power and 0.15 m/min feed speed. After the laser surface alloying, the samples were sectioned, polished and etched for optical microscopy to measure the width and depth of the melt pool.

Thermovision measurements of the Cu samples during the laser alloying were done using a ThermaCam SC640 infrared camera from FlirSystems. The initial test parameter was the oxidized copper coefficient, ranging from 0.6–0.7 (based on the emissivity table provided by the FLIR camera manufacturer). The emissivity coefficient of the tested material was selected on the basis of a test carried out with the use of a temperature meter and a heating device (a furnace equipped with a temperature controller) in which the reference samples were heated to (300, 700 and 1000) °C, respectively. Then the emissivity coefficient was calibrated to the obtained temperature measurement results. On this basis, a factor of 0.7 was selected for a temperature in the 700–1000 °C range. Temperature distributions during the laser surface alloying of the Cu samples were developed along with the recording of the cooling temperature of these samples. The sample temperature during the laser treatment was determined based on the tests. The measurement was made at a point near the melt pool and on the surface of the sample during the laser treatment process.

2.2 Mathematical model for the non-stationary heat-conduction problem

For the 3-D body made of a material that experiences solid-liquid-solid transformations, the non-stationary heat-conduction process can be described with Equation (1):¹⁷

$$\frac{\partial H}{\partial t} = \lambda \nabla^2 T + \frac{\partial Q_v}{\partial t} \quad (1)$$

where t denotes the time, T is the temperature, λ is the thermal conductivity coefficient and Q_v denotes the heat density. H denotes the volumetric enthalpy in Equation (2):

$$H(T) = \int_{T_{ref}}^T \rho c(T) dT \quad (2)$$

that depends on material density ρ and heat capacity c . T_{ref} denotes the reference temperature.

The initial condition for Equation (1) is

$$T(x, 0) = T_0(x) \Big|_{t=0} \quad x \in \Omega \quad (3)$$

where T_0 is the ambient temperature.

The following boundary conditions can be applied:

- The known heat flux q_2 on the boundary $\Gamma_2 \in \partial\Omega$, in the direction of the outward normal vector \mathbf{n} (the Neumann boundary condition):

$$q(x, t) = -\lambda \frac{\partial T}{\partial n} = q_2(x, t) \quad x \in \Gamma_2 \quad (4)$$

- The convection boundary condition on $\Gamma_3 \in \partial\Omega$, that corresponds to the heat exchange with the surrounding medium with temperature T_0 and convection coefficient h_c :

$$q(x, t) = h_c(T - T_0) \quad x \in \Gamma_3 \quad (5)$$

- The radiation boundary condition on $\Gamma_4 \in \partial\Omega$, that involves the thermal radiation coefficient ε and the Stefan-Boltzmann constant σ_b :

$$q(x, t) = \varepsilon \sigma_b (T^4 - T_0^4) \quad x \in \Gamma_4 \quad (6)$$

The problem involves phase changes and the enthalpy (Equation (2)) must be defined. One can distinguish between two cases: the mushy and isothermal phase change.²⁴ In the former case, the enthalpy is defined by:

$$H(T) = \begin{cases} \int_{T_{ref}}^T \rho c_s(T) dT & \text{for } T \leq T_s \\ \int_{T_{ref}}^{T_s} \rho c_s(T) dT + \int_{T_s}^T \rho \frac{\partial L}{\partial T} dT & \text{for } T_s < T \leq T_1 \\ \int_{T_{ref}}^{T_s} \rho c_s(T) dT + \rho L + \int_{T_1}^T \rho c_l(T) dT & \text{for } T > T_1 \end{cases} \quad (7)$$

where c_s and c_l are the heat capacities in the solid and liquid state, respectively, $(T_s - T_1)$ is the phase change temperature interval and L is the latent heat.

With the application of the Galerkin procedure (or the method of weighted residuals) and the weak formulation, the continuous initial boundary value problem described in this section is transformed into a discrete problem.¹⁸ This leads to the formulation of the finite-element method algebraic system of equations that are solved in each step of the discretized time. Due to temperature-dependent material properties, the system is non-linear and can be solved, e.g., with the Newton-Raphson method.¹⁶

2.3 Parameters of the finite element model

2.3.1 Geometry, boundary and initial conditions

The laser-alloying process using a nickel-copper coating on the copper substrate is modelled. The top surface of the model is covered with the nickel powder to form the coating. The specimen is placed on a ceramic base plate that is turning around its axis to provide the laser scanning speed v of 0.15 m/min. The laser beam scans the surface along a circular path with a radius of 15 mm, coaxial with the top surface. The width of the path is 1.5 mm. A full cycle of the alloying corresponds to the full turn of the base plate (angle $\theta = 2\pi$ rad). The geometry of the model is shown in **Figure 1**.

On the bottom face, a perfect insulation boundary condition is imposed. On the free faces (top and lateral), convection and radiation are imposed (Equations (4) and (5)). The laser beam is modelled as the heat flux

$$q_L = \frac{kP}{S} \quad (8)$$

uniformly distributed over the laser spot area. The symbols denote the following: k – the workpiece absorptance, P – the laser power, and S – the area of the laser spot. The flux q_L is imposed on an area corresponding to the spot that is moving relative to the specimen along the scanning path, with the velocity v . The laser is active for a period of $t_h = 37.7$ s. It is assumed that there is no internal heat source.

The workpiece absorptance k in Equation (8) depends on the absorptivity of the material and the angle between the surface and the laser beam. Its value can be changed to fit the simulation results to the experimental data.¹⁵ In the present work, the laser power is mainly absorbed by the nickel-powder layer. Accordingly, three values of absorptivity are considered based on the data reported in the literature. In reference²² theoretical values for the nickel powder with different geometries (hexagonal, Gaussian and bimodal) are in a range of 0.51–0.56. In the same paper, formulas for the powder absorptivity, dependent on the flat-surface absorptivity, is given. If one takes into account the values for the nickel flat surface measured by other authors,²² and apply the formulas given in reference,²⁵ the calculated powder absorptivity can exceed 0.7. In the present work, the parameter depending on the absorptivity of the top-surface material takes three values (0.56, 0.60, 0.64). The values of all the

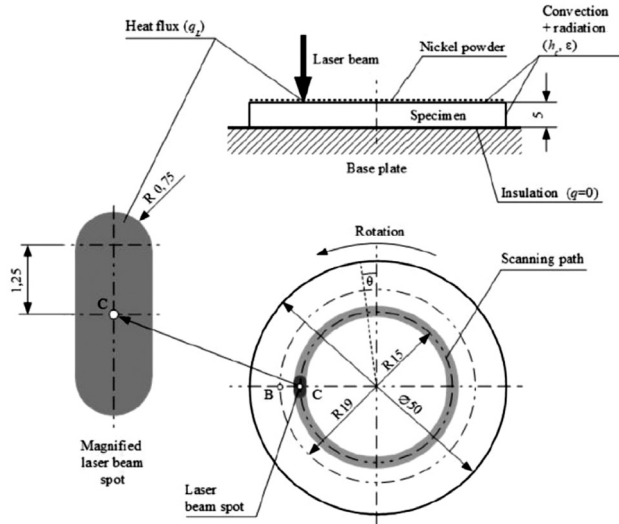


Figure 1: Geometry of the model (mm) with boundary conditions

parameters that refer to the boundary conditions are listed in Table 2.

Table 2: Boundary-condition parameters

Parameter	Value
Convection film coefficient h_c (W/(m ² ·K))	10
Ambient (initial) temperature T_0 (K)	295
Radiation coefficient (emissivity) ϵ	0.70
Workpiece absorptance k	0.56, 0.60, 0.64
Laser power P (kW)	2
Scanning speed v (m/s)	2.5×10^{-3}
Heating time t_h (s)	37.7

2.3.2 Material model parameters

The copper material basic parameters are included in the applied FEM software. However, to model the material behaviour in a broader range of temperature, the data are complemented with temperature-dependent material properties. The properties of copper up to the melting point are available in reference.²⁶ In the present calculations, it is assumed that the material properties above the melting point remain constant. The specifications of the basic material parameters is given in Table 3.

Table 3: Material model parameters

Parameter	Value
Density ρ (kg/m ³)	8978
Latent heat of fusion L (J/kg)	205×10^3
Thermal conductivity $\lambda(T)$ (W/(m·K))	tabular ²⁶
Specific heat $c(T)$ (J/(kg·K))	tabular ²⁶
Melting temperature T_1 (K)	1 356

For the enthalpy calculations, the mushy phase-change model is applied, having a narrow range of the phase-change temperature ($T_s = 1356$ K, $T_l = 1361$ K) that allows one to avoid numerical instabilities during the solving process.²⁴ The tabular data for the enthalpy are listed in Table 4. The points are used to the linear inter-

polation of the data in three characteristic temperature intervals defined by Equation (7).

Table 4: Enthalpy tabular data

Temperature T (K)	Enthalpy $H(T)$ (J/m ³)
293	10^3
1 356	5×10^9
1 361	6.84×10^9
2 500	12.10×10^9

2.3.3 Geometry and time discretization

To minimize the geometry discretization effect, a high-quality mesh is applied, composed of 8-node hexahedral elements as its major part. Linear shape functions are applied to reduce the computation time. The mesh is densified in the region of the high-temperature gradient.

The position of the specimen is fixed and the moving heat flux q_L is applied by an APDL (ANSYS Parametric Design Language) script. The script selects the nodes that are located in the laser spot area. The area moves along the scanning path with the rotation of a local coordinate system at an angle corresponding to a single time step. The heating time t_h corresponds to the move of the laser spot along the full scanning path ($\theta = 2\pi$). The time is divided into 800 equal time steps that correspond to the angle increments of the laser spot movement or, equivalently, the rotation of the specimen with a fixed laser spot in the laboratory experiment.

3 RESULTS AND DISCUSSION

The temperature distribution in the workpiece is calculated. The distribution for the selected time corresponding to four values of θ (0.5, 1, 1.5 and 2π) and the highest value of the workpiece absorptance ($k = 0.64$) is shown in Figure 2. The temperature distribution is characteristic for laser treatment processes. The temperature increases with the time in the whole volume of the specimen. High temperature values and high gradients occur near the area of the laser spot. The volume with a temperature greater than T_1 , corresponding to the melt pool, is filled up with white colour. It moves along the scanning path and its size increases in time. The maximum size is observed at the end time ($t = 37.7$ s). The temperature at point B is measured using the thermographic camera and compared to the FEM results. Figure 3 shows the temperature plot versus time.

The FEM models initially underestimate the measured temperature (Figure 3). However, for the simulations and experiment, the trends are similar. For the measurements, high fluctuations can be observed that can be caused by the non-uniform thickness of the Ni powder layer and thus its variable absorptance. These fluctuations are not observed in the simulation results. At the end time, the measured temperature is placed between the FEM with $k = 0.60$ and $k = 0.64$. The smallest rela-

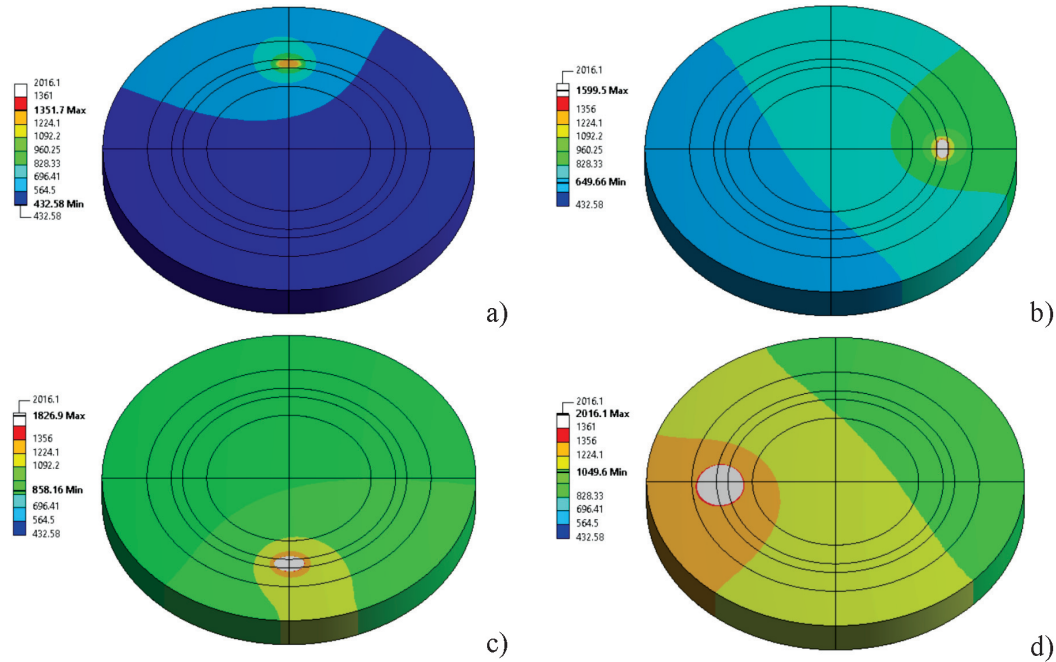


Figure 2: Simulated temperature distribution for $k = 0.64$: a) $\theta = 0.5\pi$, b) $\theta = 1\pi$, c) $\theta = 1.5\pi$, d) $\theta = 2\pi$

tive difference in the measurement is observed for FEM with $k = 0.60$ and is about 1.2 %. For $k = 0.64$, the difference is about 4.3 %. At the simulation end time, the temperature of point B is close to the melting temperature of pure copper. From the temperature distribution near the laser spot, one can deduce the melt pool shape and dimensions. The width and depth of the pool can be measured experimentally after the process, by taking microscopic images of the selected sections of a specimen. Here, such images are taken in planes including points B and C. The sections correspond to $\theta = 1.5\pi$ and 2π . The simulated temperature distributions for $k = 0.64$ are shown in Figures 4a and 4b. Selected numerical data from the simulations and experiment are collected in Table 5. The data include the maximum temperature at

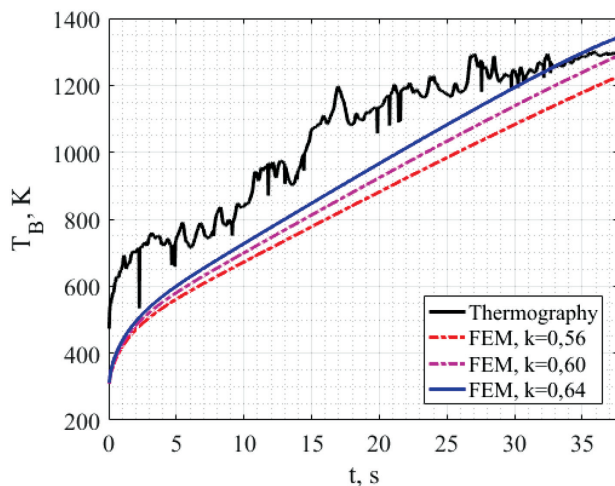


Figure 3: Temperature at point B versus time

point B and melt pool dimensions. The dimensions are also compared in Figures 5a and 5b, for $\theta = 1.5\pi$ and 2π , respectively. In the figures, the microscopic images are shown.

Table 5: Simulation and experiment results – maximum temperature at point B and melt pool dimensions

Method	Max (T_B), K	Melt pool width (mm)		Melt pool depth (mm)	
		$\theta = 1.5\pi$	$\theta = 2\pi$	$\theta = 1.5\pi$	$\theta = 2\pi$
FEM, $k = 0.56$	1 227	1.8	3.3	0.6	1.5
FEM, $k = 0.60$	1 289	2.2	4.5	0.9	2.3
FEM, $k = 0.64$	1 343	2.7	6.3	1.2	3.5
Experiment	1 304	2.7	7.7	0.9	3.2

The width and depth of the measured melt pool for two different cross-sections are generally placed between the FEM results for the workpiece absorptance of $k = 0.60$ and 0.64 . Only simulated depth for $k = 0.64$

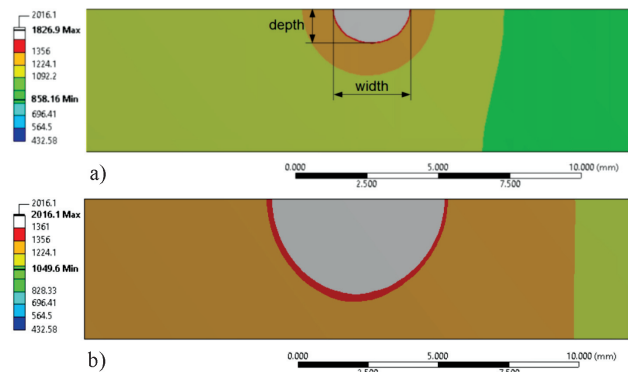


Figure 4: Simulated melt-pool cross-section for $k = 0.64$ and: a) $\theta_1 = 1.5\pi$, b) $\theta_2 = 2\pi$

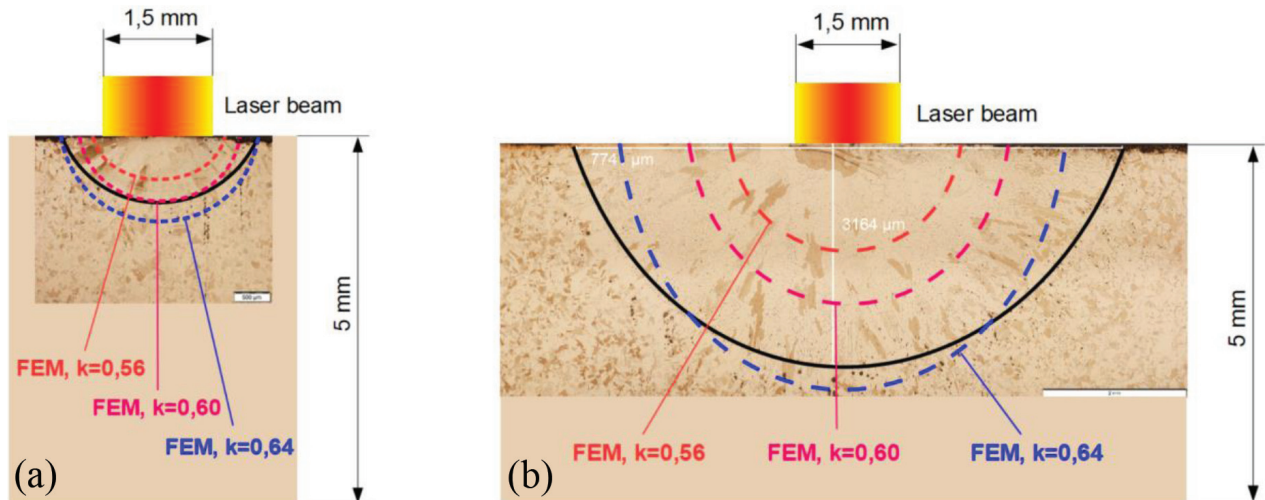


Figure 5: Comparison between the measured and simulated melt pool: a) $\theta_1 = 1.5\pi$, b) $\theta_2 = 2\pi$

slightly exceeds the measured value. The maximum difference between dimensions of the actual and simulated melt pool for $k = 0.64$ does not exceed 1.5 mm. Such a value can be considered acceptable in simulations if one takes into account the width of the laser beam (1.5 mm) and the maximum width of the melt pool (7.7 mm), **Figure 5b**). Thus, the developed model can be used in the identification of the workpiece absorptance. Here, the identified absorptance is in the interval of 0.60–0.64. Such values are close to the Ni powder absorption coefficients reported in the literature.²²

4 CONCLUSIONS

In this work, a computer model for the prediction of the temperature distribution in the surface laser alloying of pure copper with Ni powder is developed. To the simulation, the ANSYS finite element code is applied. The phase transformation is taken into account by varying the enthalpy. To simplify the model, typical assumptions are introduced, e.g., a still melt pool with constant properties. The domain of the powder is not discretized. Instead, its absorptance is taken into account when moving the heat-flux boundary condition in the area of the moving laser spot. Approximate absorptance of the workpiece is identified by comparing the simulated temperature and melt pool size with the experimental data. Laboratory measurements show that the melt pool increases through the process. The computational model gives results that correlate with the experimental data. Thus, the model can be used to control the melt pool size along the scanning path. This can be achieved by changing the laser power through the laser surface alloying process. To improve the model, more phenomena should be considered, e.g., the liquid flow in the melt pool, evaporation of the material, interaction with the shield gas, and others. However, one can expect that such improvements will substantially increase the computation

time. Despite the rigorous assumptions, the present model gives acceptable results.

Acknowledgment

This research was carried out as a part of the project financed by the National Centre for Research and Development of Poland, project number LIDER/33/0091/L-7/NCBR/2016 and partially within the framework of the statutory subsidy of the Department of Computational Mechanics and Engineering, Silesian University of Technology, Poland.

5 REFERENCES

- J. R. Davis, ASM Specialty Handbook. Copper and Copper Alloys, ASM International, 2001
- Z. Rdzawski, Alloyed copper, Silesian University of Technology, Gliwice 2009, 229
- T. Wierchoń, Structure and properties of multicomponent and composite layers produced by combined surface engineering methods, Surf. Coat. Technol., 180–181 (2004), 458–464, doi:10.1016/j.surfcoat.2003.10.090
- D. Janicki, Microstructure and sliding wear behavior of in-situ TiC-reinforced composite surface layers fabricated on ductile cast iron by laser alloying, Materials, 11 (2018) 75, doi:10.3390/ma11010075
- A. Lisiecki, Study of Optical Properties of Surface Layers Produced by Laser Surface Melting and Laser Surface Nitriding of Titanium Alloy, Materials, 12 (2019) 19, 3112, doi:10.3390/ma12193112
- J. Kusinski, S. Kac, A. Kopia, A. Radziszewska, M. Rozmus-Górnikowska, B. Major, L. Major, J. Marczak, A. Lisiecki, Laser modification of the materials surface layer – a review paper, Bulletin of the Polish Academy of Sciences: Technical Sciences, 60 (2012), 711–728
- F. Liu, Ch. Liu, S. Chen, X. Tao, Z. Xu, M. Wang, Pulsed Nd:YAG laser post-treatment Ni-based crack-free coating on copper substrate and its wear properties, Surf. Coat. Technol., 201 (2007), 6332–6339, doi:10.1016/j.surfcoat.2006.11.038
- F. Liu, L. Changsheng, Ch. Suiyuan, T. Xingqi, Z. Yong, Laser cladding Ni-Co duplex coating on copper substrate, Opt. Laser Eng., 48 (2010) 7–8, 792–799, doi:10.1016/j.optlaseng.2010.02.009

- ⁹ G. Dehm, M. Bamberger, Laser cladding of Co-based hardfacing on Cu substrate, *J. Mater. Sci.*, 37 (2002), 5345–5353, doi:10.1023/A:1021041527980
- ¹⁰ K. W. Ng, H. C. Man, F. T. Cheng, T. M. Yue, Laser cladding of copper with molybdenum for wear resistance enhancement in electrical contacts, *Appl. Surf. Sci.*, 253 (2007) 14, 6236–6241, doi:10.1016/j.apsusc.2007.01.086
- ¹¹ S. Bysakh, K. Chattopadhyay, T. Maiwald, R. Galun, B. L. Mordike, Microstructure evolution in laser alloyed layer of Cu-Fe-Al-Si on Cu substrate, *Mater. Sci. Eng. A*, 375–377 (2004), 661–665, doi:10.1016/j.msea.2003.10.263
- ¹² J. Domagała-Dubiel, W. Głuchowski, Z. Rdzawski, D. Janicki, A. Kowalski, K. Bilewska, Microstructure analysis and mechanical properties of copper after laser surface treatment, *Proc. of EMC 2019, European Metallurgical Conference 4*, 2019, 1529–1539
- ¹³ F. Bachmann, Industrial applications of high-power diode lasers in materials processing, *Appl. Surf. Sci.*, 229 (2003) 208–209, 125–136, doi:10.1016/S0169-4332(02)01349-1
- ¹⁴ S. Barnes, N. Timms, B. Bryden, et al., High power diode laser cladding, *J. Mater. Process. Technol.*, 138 (2003), 411–416, doi:10.1016/S0924-0136(03)00109-2
- ¹⁵ B. De La Batut, O. Fergani, V. Brotan, M. Bambach, M. El Mansouri, Analytical and Numerical Temperature Prediction in Direct Metal Deposition, *J. Manuf. Mater. Process.*, 1 (2017) 3, doi:10.3390/jmmp1010003
- ¹⁶ K. J. Bathe, *Finite element procedures*, Prentice Hall, Pearson Education, Inc., Watertown, UK, 2014
- ¹⁷ Z. Luo, Y. Zhao, A survey of finite element analysis of temperature and thermal stress fields in powder bed fusion Additive Manufacturing, *Addit. Manuf.*, 21 (2018), 318–332, doi:10.1016/j.addma.2018.03.022
- ¹⁸ O. C. Zienkiewicz, R. L. Taylor, *The finite element method*, Butterworth-Heinemann, Oxford, UK, 2000
- ¹⁹ E. Majchrzak, J. Dziatkiewicz, Ł. Turchan, Analysis of thermal processes occurring in the microdomain subjected to the ultrashort laser pulse using the axisymmetric two-temperature model, *Int. J. Multiscale Comput. Eng.*, 15 (2017) 5, 395–411, doi:10.1615/IntJMultCompEng.2017020480
- ²⁰ E. Majchrzak, Ł. Turchan, Modeling of laser heating of bi-layered microdomain using the general boundary element method, *Eng. Anal. Bound. Elem.*, 108 (2019), 438–446, doi:10.1016/j.enganabound.2019.09.005
- ²¹ E. Majchrzak, General Boundary Element Method for the Dual-Phase Lag Equations Describing the Heating of Two-Layered Thin Metal Films, In: A. Öchsner, H. Altenbach (eds.), *Engineering Design Applications II, Advanced Structured Materials*, Springer, Cham 2020, 263–278, doi:10.1007/978-3-030-20801-1_20
- ²² C. D. Boley, S. C. Mitchell, A. M. Rubenchik, S. S. Q Wu, Metal powder absorptivity: modeling and experiment, *Appl. Opt.*, 55 (2016) 23, 6496–6500, doi:10.1364/AO.55.006496
- ²³ M. Bonek, A. Sliwa, J. Mięka, Computer simulation of the relationship between selected properties of laser remelted tool steel surface layer, *Appl. Surf. Sci.*, 388 (2016), 174–179, doi:10.1016/j.apsusc.2016.01.256
- ²⁴ B. Nedjar, An enthalpy-based finite element method for nonlinear heat problems involving phase change, *Comput. Struct.*, 80 (2002) 1, 9–21, doi:10.1016/S0045-7949(01)00165-1
- ²⁵ R. Indhu, V. Vivek, L. Sarathkumar, A. Bharatish, S. Soundarapandian, Overview of Laser Absorptivity Measurement Techniques for Material Processing, *Lasers Manuf. Mater. Process.*, 5 (2018), 458–481, doi:10.1007/s40516-018-0075-1
- ²⁶ P. J. Karditsas, M. J. Baptiste, *Thermal and Structural Properties of Fusion Related Materials*, UKAEA FUS 294, 1995, <http://www-ferp.ucsd.edu/LIB/PROPS/PANOS/matintro.html> (accessed February 7, 2020)